

LA-UR-13-27544

Approved for public release; distribution is unlimited.

Title: JET FORMATION IN CERIUM METAL TO EXAMINE MATERIAL STRENGTH

Author(s): Jensen, Brian J.; Cherne, Frank J.; Prime, Michael B.; Fezzaa, Kamel;
Iverson, Adam J.; Yeager, John D.; Carlson, Carl A.; Ramos, Kyle J.;
Hooks, Daniel E.; Cooley, Jason C.; Dimonte, Guy

Issued: 2015-03-20 (Rev.1) (Draft)

Jensen, B. J., Cherne, F. J., Prime, M. B., Fezzaa, K., Iverson, A. J., Carlson, C. A., Yeager, J. D., Ramos, K. J., Hooks, D. E., Cooley, J. C., and Dimonte, G., 2015, "Jet formation in cerium metal to examine material strength," J. Appl. Phys., 118(19), p. 195903.

Disclaimer:

Los Alamos National Laboratory, an affirmative action/equal opportunity employer, is operated by the Los Alamos National Security, LLC for the National Nuclear Security Administration of the U.S. Department of Energy under contract DE-AC52-06NA25396. By approving this article, the publisher recognizes that the U.S. Government retains nonexclusive, royalty-free license to publish or reproduce the published form of this contribution, or to allow others to do so, for U.S. Government purposes. Los Alamos National Laboratory requests that the publisher identify this article as work performed under the auspices of the U.S. Department of Energy. Los Alamos National Laboratory strongly supports academic freedom and a researcher's right to publish; as an institution, however, the Laboratory does not endorse the viewpoint of a publication or guarantee its technical correctness.

JET FORMATION IN CERIUM METAL TO EXAMINE MATERIAL STRENGTH

B.J. Jensen,* F.J. Cherne, and M.B. Prime

Los Alamos National Laboratory, Los Alamos NM 87545, USA

K. Fezzaa

Argonne National Laboratory, Argonne, Illinois 60439, USA

A.J. Iverson and C.A. Carlson

National Security Technologies LLC, Los Alamos, NM 87544, USA

J.D. Yeager, K.J. Ramos, D.E. Hooks, J.C. Cooley, and G. Dimonte

Los Alamos National Laboratory, Los Alamos NM 87545

Abstract

Examining the evolution of material properties at extreme conditions advances our understanding of numerous high-pressure phenomena from natural events like meteorite impacts to general solid mechanics and fluid flow behavior. Recent advances in synchrotron diagnostics coupled with dynamic compression platforms have introduced new possibilities for examining in-situ, spatially resolved material response with nanosecond time resolution. In this work, we examined jet formation from a Richtmyer-Meshkov instability in cerium initially shocked into a transient, high-pressure phase, and then released to a low-pressure, higher-temperature state. Cerium's rich phase diagram allows us to study the yield stress following a shock induced solid-solid phase transition. X-ray imaging was used to obtain images of jet formation and evolution with 2-3 μm spatial resolution. From these images, an analytic method was used to estimate the post-shock yield stress, and these results were compared to continuum calculations that incorporated an experimentally validated equation-of-state (EOS) for cerium coupled with a deviatoric strength model. Reasonable agreement was observed between the calculations and the data illustrating the sensitivity of jet formation on the yield stress values. The data and analysis shown here provide insight into material strength during dynamic loading which is expected to aid in the development of strength aware multi-phase equations-of-state (EOS) required to predict the response of matter at extreme conditions.

I. INTRODUCTION

The ability to understand the evolution of material properties at extreme conditions is of significant interest within the dynamic high-pressure community, and is relevant to fields ranging from fundamental condensed matter physics to general solid and fluid flow behavior. These “extreme” states of matter, found in nature during meteorite impacts¹⁻³ or within the earth’s core,^{4,5} can be created in the laboratory on short timescales (picoseconds to microseconds) using shock waves generated by explosives, lasers, and impact systems. By studying how the shock wave propagates through a material, traditional measurements have provided insight into various phenomena including elastic-plastic deformation,^{6,7} shock-induced phase transitions,⁸⁻¹⁰ equation-of-state, and material strength.¹¹⁻¹³ In particular, the ability to examine material strength during high strain-rate, dynamic deformation, in both compression and tension, remains a significant scientific challenge because of the difficulty in generating well-defined loading conditions. Furthermore, a material’s strength is likely dependent on the details and evolution of the microstructure which is difficult to diagnose. Rayleigh-Taylor instabilities (RTI) have long been used to infer material strength¹⁴⁻¹⁸ and recently have been instrumental in developing sophisticated constitutive models for the high-pressure, high-rate, shockless regimes accessed in such experiments.^{19,20} In contrast, Richtmyer-Meshkov instabilities (RMI) are formed when a shock wave interacts with a perturbation at an interface, and have shown a sensitivity to strength in the post-shock state.^{12,21,22} Although RMI theory is less developed than RTI, RMI experiments can provide a unique data set to inform constitutive models intended to predict material behavior over a wide range of loading conditions.

In this work, we perform RMI growth experiments²³ using the free surface configuration to estimate the tensile yield stress for cerium following a high-pressure, shock-induced phase transition. Instabilities, or jets, were imaged using state-of-the-art X-ray imaging capabilities coupled to an impact system now available at the Advanced Photon Source.^{24,25} Cerium metal was an ideal choice for examining phase dependent strength because it exhibits a rich and complex phase diagram (see Fig. 1) at relatively moderate pressures and temperatures readily accessible using standard high pressure techniques. First studied by Bridgman in the 1920s,²⁶ cerium has a well-known solid-solid critical point (CP), four known phases at zero pressure, several higher pressure solid phases, and an anomalous melt boundary.²⁷⁻³⁰

The low pressure γ (fcc) phase is known to be anomalous, characterized by a negative bulk modulus derivative³¹, and the isostructural transition to the α (fcc) phase at approximately 0.75 GPa is accompanied by a large 13-16 percent volume collapse.^{26,32,33} Above the CP, the γ - α transition is continuous (in volume) with no change in atomic structure though there are changes in the compressibility. Above 4 GPa, a complex region has been observed consisting of the α' (oC4) and α'' (mC4) phases followed by the ϵ (bct) phase above 13.5 GPa which exists up to Mbar pressures.^{27,34-36} At higher temperatures (greater than 600 K and below the melt boundary), a direct α to ϵ transition has been reported although there are disagreements in both slope and location of the boundary.³⁶⁻³⁸ During shock wave loading, the Hugoniot passes through the γ phase, α phase, and into the liquid (red curve in Fig. 1). Sound speed data on the Hugoniot have shown that cerium begins to melt at approximately 10.2 GPa with no indication of a transition to the ϵ phase within the 5-10 GPa pressure range.¹⁰ Shock loading experiments in the γ - α region of the phase diagram³³ confirm the location of the phase boundary, the associated volume collapse, and the critical point as compared with static data.³¹ All experiments in this work were performed in the γ - α region of the phase diagram where there exists an experimentally informed multi-phase equation-of-state^{39,40} (EOS) that can sufficiently describe the continuum response during loading.

The experimental methods and results are presented in Section II and III, respectively, followed by the data analysis and discussion in Section IV. The conclusions are summarized in Section V.

II. EXPERIMENTAL METHODS

Shock waves were generated in the cerium sample (Fig. 2) using the IMPact System for Ultrafast Synchrotron Experiments (IMPULSE) located at Sector 32 ID-B of the Advanced Photon Source (Argonne, IL).^{24,25} IMPULSE is a gas-gun system used to launch projectiles at targets which is specifically designed to couple with the X-ray beam at a synchrotron source. Projectiles with copper impactors are accelerated down the gun barrel to impact the cerium located in an evacuated target chamber (< 100 millitorr) and positioned in the X-ray beam. After impact, a shock wave propagates through the cerium sample transforming it from the ambient γ phase into the higher pressure α phase. Subsequently, the shock wave

interacts with the grooves and reflects from the back of the cerium sample (which is at zero pressure) generating a release wave that transforms the material back into the γ phase. These three states that define the loading path are shown in Fig. 1 on the cerium phase diagram as states A (ambient state), B (shocked state), and C (released state), respectively. Metal jets form at the groove locations (Fig. 2) from the cerium sample which is now in a low-pressure, higher temperature state in the γ phase (state C). By measuring the jet height as a function of time combined with the velocity histories for a range of impact stresses, the yield stress can be estimated for cerium following reversion to the γ phase. Note that a minimum impact stress of 5 GPa was chosen to put the shocked state (e.g., state B) well into the α phase and ensure that the release path exceeded the critical point (CP). Following a release path below CP would result in an additional discontinuous volume change associated with the reverse isostructural $\alpha - \gamma$ transition.

X-ray imaging was used to obtain time-resolved images of jet formation (Fig. 2 inset) with 2-3 μm spatial resolution. During the experiment, a series of 80-ps width X-ray bunches spaced 153.4 nanoseconds apart interacted with the sample and then illuminated a LuAg scintillator. The scintillator converted the X-rays to visible light which is optically coupled to four image intensified charge coupled device (ICCD) detectors. Because cerium is opaque to the 12-13 KeV X-rays used here, the jet and free surface interfaces are clearly visible and can be tracked as a function of time. Photonic Doppler Velocimetry (PDV)⁴¹ probes were used to measure the jet velocity, the free-surface velocity, and the projectile velocity at impact⁴² simultaneously. High-purity cerium samples (99.99%) similar to those used in past work¹⁰ were used for all experiments with a nominal ambient density of $6.687 \pm 1\%$ g/cc and an approximate 50 μm grain size. The cerium samples were nominally 1.25 mm in thickness and 9 mm in diameter. Because cerium oxides readily in air, the sample was machined and target assembled within approximately one hour of the experiment. During that time, the assembled target was stored in a container with a desiccant material. Further details of the experiment setup and timing, and the X-ray imaging technique are described elsewhere.^{24,25,43}

III. EXPERIMENTAL RESULTS

A total of five experiments were performed with impact stresses ranging from 5.30 to 7.64 GPa. The relevant experimental quantities are reported in Table I. Grooves were machined in the back surface of the cerium sample with groove depths, h_0 , ranging from 0.051 mm to 0.127 mm with a wavelength (distance between grooves) of $\lambda = 0.457$ mm. The groove depths and wavelengths were chosen so that the jet height converged to a constant value with time, defined as “saturation”, and moved at the same velocity as the free surface of the sample. Example data obtained for one of the experiments (shot 13-030) are shown in Fig. 3-A. In this experiment, a copper flyer impacted a cerium sample at a projectile velocity of 0.629 km/s for a peak impact stress in the cerium of 5.62 GPa. The X-ray image (Fig. 3-A) shows multiple frames obtained from the four detectors for a single experiment plotted together in the image with the interfaces highlighted for clarity. The corresponding PDV data are shown (Fig. 3-B) where the particle velocity (km/s) is plotted versus time (μ s). Following shock arrival near $t = 0$ μ s, two distinct velocity histories were visible, corresponding to the jet and the free-surface velocities, respectively. The jet history shows a sharp rise followed by a rapid decrease to the steady state free surface value. The images were taken as the jet and free surface velocities converged at the saturation point. The images obtained for all five experiments are summarized in Fig. 3-C. The first three images show that, for constant kh_0 values (where the wave number, k , equals $2\pi/\lambda$), an increase in the impact stress leads to a decrease in the jet width. The last two images show that, for similar impact stresses, an increase in the kh_0 values increases the time required to arrest the jet growth leading to a greater jet height.

IV. ANALYSIS AND DISCUSSION

We estimated the yield stress from the Richtmyer-Meshkov instability growth using several methods. The first two methods used the formalism developed by Dimonte et al.¹² to determine the yield stress, Y , from the jet velocity history obtained from the PDV data. The yield stress is given by the equation¹²

$$Y \sim 0.24\rho_A \frac{|V_{sp}^0|^2}{kh_{sp}^{max}} \quad (1)$$

where ρ_A is the ambient density of the cerium sample, V_{sp}^0 is the peak jet growth rate defined as the difference between the maximum jet and the free-surface velocities, and h_{sp}^{max} is the maximum jet amplitude at saturation. The geometric factor of 0.24 was based on a sinusoidal perturbation which is an approximation of the groove geometry used in this work.¹² The first method used the velocity histories to calculate the quantity kh_{sp}^{max} defined by the equation

$$kh_{sp}^{max} = kh_0^+ + k \int V_{sp}(t) dt \quad (2)$$

where kh_0^+ is given by $kh_0^-(1 - u_{fs}/U_s)$ and $V_{sp}(t)$ is the time history of the velocity difference between the jet velocity and the free surface velocity (given by the PDV data). The quantities h_0^- and h_0^+ are the pre-shocked and shocked groove depths, respectively. The free-surface particle velocity, u_{fs} , and the shock velocity in the cerium sample, U_s , were determined using available data on cerium combined with the Rankine-Hugoniot relations. The yield stress calculated in this way is defined as Y_{vel} . The second method took advantage of the high spatial resolution of the X-ray images to estimate h_{sp}^{max} directly from the data. This allowed us to avoid the uncertainties associated with the shock parameters U_s and u_{fs} and the integration of the velocity histories according to Equation 2. An edge finding algorithm was used to locate the cerium-vacuum interface in each image, and the difference between the jet peak and the trailing free surface was taken as the jet height, or h_{sp}^{max} . Equation 1 was then used to calculate the yield stress, Y_{image} .

Equation (1) for yield stress was developed for materials with a linear $U_s - U_p$ Hugoniot. The nonlinear behavior of cerium associated with the γ, α region of the phase diagram is inconsistent with such an assumption, and could reasonably be expected to have a significant influence on the hydrodynamics of the instability growth and arrest. To account for these effects, a third approach was used to estimate the yield stress. Continuum simulations were performed using FLAG, a Lagrangian hydrodynamics code.^{44,45} Each simulation used a two-dimensional plane strain mesh that spanned two full wavelengths of the perturbation and had periodic boundary conditions to enforce cyclic symmetry (see Fig. 4-A). The mesh consisted of zones approximately 10 μm on a side for about 42,000 zones total in the domain. The copper impactor was modeled using a tabular equation of state and a Preston-Tonks-Wallace deviatoric strength model.⁴⁶ The cerium target was modeled using a modified version⁴⁰ of the EOS presented by Elkin, et.al.³⁹ The modifications adjusted the $\gamma - \alpha$ phase boundary to better capture the phase transition characteristics and the behavior of the bulk modulus

near the phase transition.³¹ To compare with the analytic estimates of yield stress, deviatoric strength was modeled using the same assumption of elastic-plastic behavior with a constant yield/flow stress. A predictive constitutive strength model for high-rate problems¹⁹ is beyond the scope of this paper, and a more sophisticated treatment would be required to make use of these data to calibrate such a model. The constant strength model is sufficient to extract an average yield stress that is consistent with the experiments. In the simulations, the copper was initially moving at the impact velocity and at $t = 0$ impacted the cerium. Depending on the yield stress values used in the simulations, the jet growth generally arrested in under two microseconds from shock breakout, but the simulation continued for several microseconds.

For a given experiment, the yield stress was adjusted iteratively in the simulations until the arrested jet height matched the data. An example calculation for shot 13-030 (Fig. 4) shows the simulation results for three values of Y all plotted at 900 nanoseconds after shock breakout when the jet has arrested. With $Y_{sim} = 0.13$ GPa (Fig. 4-C), the jet height matches the observed value (see Fig. 3). The simulation indicates strain rates from $1 - 4 \times 10^6$ /sec during jet growth and arrest, and an accumulated equivalent plastic strain of about 120% in the jet. With Y decreased to half (Fig. 4-D), the final jet height increases to 240% of the observed value and with Y doubled (Fig. 3-b), the final jet height is only 24% of the observed value. Velocimetry histories obtained from the calculation (Fig. 3-b) are in reasonable agreement with the experimental data. Considering the lack of strength data in this strain rate regime, and the associated difficulties developing physically based strength models, such sensitivity to the yield stress is very encouraging.

All experimental parameters and quantities are summarized in Table I. The projectile velocity, V_p , and the initial groove depths are shown in column 2 and 3, respectively. The peak longitudinal stress and the density in the cerium calculated using available data¹⁰ are shown in column 6 and 7, respectively. The temperatures for the shocked state, T_B , and the release state, T_C , were calculated using the EOS. These values are shown in columns 8 and 9, respectively. Values for Y are shown in columns 10 through 12. Estimated uncertainties are listed in the table and standard error propagation was used to estimate the uncertainties in the yield stress values. All results for the yield stress show reasonably good agreement, but the use of images to directly measure the jet height resulted in a 50% decrease in experimental uncertainty. As noted earlier, by using the imaging diagnostic to directly measure the jet height, we could eliminate the uncertainty associated with U_s and u_{fs} shock parameters.

The calculated results (Table I; column 12) generally fall within 13% of estimated values using the simple analytical approximation in spite of the simplifying assumptions used to derive Equations 1 and 2. Overall, the yield stress shows a decrease in value from 0.15 to 0.11 GPa as the post-release temperature increases from about 478 to 557 degrees K (Table I; column 9) for peak compressed states of 5.62 to 7.64 GPa.

RMI experiments have been largely limited to the study of elastic-plastic deformation in shocked solids.^{12,47} For example, past work used an explosive drive to launch a non-steady shock wave into a copper sample to examine jet formation during plastic deformation. Proton radiography was used to capture images of the jets and PDV to measure the jet velocities. Although radiographic images were obtained showing the jet formation, the spatial resolution was not sufficient to estimate the jet height directly from the data. Because of this, Eq.(2) was used to calculate the jet height by integrating the jet velocity histories followed by application of Eq.1 to estimate the yield stress. In the current work, we performed similar RMI experiments using a gas gun system to generate a steady shock wave in cerium to measure the yield stress following a shock-induced solid-solid phase transition. The jet evolution was diagnosed using X-ray imaging with micrometer spatial resolution and PDV to measure the jet velocities. Yield stress values were obtained from the data using three methods: (1) application of Eq.1 using the jet height measured directly from the X-ray images, (2) integration of the jet velocity as described in Eq.2, and (3) by comparing the X-ray images with simulated images obtained from a hydrocode that included a cerium EOS and a simple strength model with a variable yield stress. The yield stress values obtained using these three different methods were in reasonable agreement.

It is important to note that the yield stress values provided by the RMI method correspond to a tensile state the develops after shock cycling the material. This can be seen in the following FLAG simulations that were performed for cerium to examine the evolution of the jet during the RMI experiment. The results are shown in Fig. 5 for parameters consistent with shot 13-030. In Fig. 5-A, the shock wave is shown as it arrives at the cerium-vacuum interface and begins interacting with the bottom of the groove. The stress state behind the shock front is approximately 5.2 GPa consistent with the material being in the α phase. Prior to significant evolution of the jet (Fig. 5-B through D), the shock wave reflects from the cerium-vacuum interface, and the material releases from the Hugoniot state to low pressure (note that the cerium-vacuum interface is always at a zero pressure state). The release path

shown in Fig. 1 extends from the Hugoniot (α phase) to low-pressure (γ phase) exceeding the critical point where the reversion from the α to γ is continuous (no volume change). The final release state from which the jet begins to form is in the low-pressure γ phase though at higher residual temperatures between 478 and 557 degrees K. This is a key finding, and illustrates the advantage of using hydrodynamic simulations to complement the high fidelity experimental data obtained using the X-ray PCI diagnostic. Furthermore, this means that although the yield stress is likely affected by microstructural changes caused by plastic deformation (in the copper experiments) or the phase transition (in the cerium experiments), conclusions about the evolution of strength and correlations with the microstructure, in particular, during loading are not possible using RMI experiments alone. To this end, efforts are underway to examine material strength in the initial peak shocked state (point B in Fig. 1) using the double-shock method¹³ and X-ray diffraction.⁴⁸ Additional RMI experiments on cerium with different grain size are in progress to examine the effect of the initial cerium grain size on the yield stress. In this way, data will be obtained throughout the loading process providing insight into the evolution of strength.

V. SUMMARY

In conclusion, we have used the high spatial and temporal resolution of X-ray imaging coupled to an impact system at the Advanced Photon Source to study jet formation in cerium metal. By measuring the jet velocity and obtaining X-ray images of the jets as they evolved, we were able to estimate the yield stress in tension for a material that was initially shock-cycled through a solid-solid phase transition and then released to a high-temperature state back in the γ phase. The experimental data were compared to continuum calculations that included an experimentally validated, multi-phase EOS for cerium to account for the phase transition and the nonlinear response in the $\gamma - \alpha$ region. Overall, the experimental and calculated results were in reasonable agreement, and the data show that the yield stress of cerium decreased by approximately 30 percent, from 0.15 to 0.11 GPa, as the peak impact stress in the sample increased from 5.62 to 7.64 GPa. Furthermore, the uncertainty was observed to decrease by approximately 50 percent for yield stress values calculated using the X-ray images. Work is underway to continue the study of material strength for a phase transforming solid by applying the reshock method reported previously¹³ combined with

X-ray diffraction techniques^{7,48,49} to examine strength in the high pressure α phase prior to release. We expect that the data shown here coupled with future work will continue provide insight into underlying mechanisms governing material strength which will aid in the development of physically based, strength-aware multi-phase equation-of-state models for materials that are required to predict and control the response of matter at extreme conditions.

VI. ACKNOWLEDGMENTS

This work was performed at Los Alamos National Laboratory and at Argonne National Laboratory's Advanced Photon Source (APS). Charles Owens and Tim Pierce (LANL) are gratefully acknowledged for technical assistance with target and projectile fabrication, gun setup, and shot execution. A. Deriy (Argonne National Laboratory) is thanked for technical support at Sector 32 of the APS. This work was supported by LANL's MaRIE concept and Science Campaign programs. Yeager was supported by an Agnew National Security Postdoctoral Fellowship. LANL is operated by Los Alamos National Security, LLC for the U.S. Department of Energy (DOE) under Contract No. DE-AC52-06NA25396. Use of the Advanced Photon Source, an Office of Science User Facility operated for the DOE Office of Science by Argonne National Laboratory, was supported by the U.S. DOE under Contract No. DE-AC02-06CH11357.

REFERENCES

- * bjjensen@lanl.gov
- ¹ H. J. Melosh, *Icarus* **59**, 234 (1984).
 - ² W. U. Reimold, *Science* **300**, 1889 (2003).
 - ³ C. A. Trepmann, *Earth Planet. Sc. Lett.* **267**, 322 (2008).
 - ⁴ A. Laio, S. Bernard, G. L. Chiarotti, S. Scandolo, and E. Tosatti, *Science* **287**, 1027 (2000).
 - ⁵ C. S. Yoo, N. C. Holmes, M. Ross, D. J. Webb, and C. Pike, *Phys. Rev. Lett.* **70**, 3931 (1993).
 - ⁶ J. R. Asay, G. R. Fowles, G. E. Duvall, M. H. Miles, and R. F. Tindler, *J. Appl. Phys.* **43**, 2132 (1972).
 - ⁷ B. J. Jensen and Y. M. Gupta, *J. Appl. Phys.* **104**, 013510 (2008).
 - ⁸ D. H. Dolan, M. D. Knudson, C. A. Hall, and C. Deeney, *Nat. Phys. Lett.* **3**, 339 (2007).
 - ⁹ B. J. Jensen, G. T. Gray, and R. S. Hixson, *J. Appl. Phys* **105**, 103502 (2009).
 - ¹⁰ B. J. Jensen, F. J. Cherne, J. C. Cooley, M. V. Zhernokletov, and A. E. Kovalev, *Phys. Rev. B* **81**, 214109 (2010).
 - ¹¹ H. Huang and J. R. Asay, *J. Appl. Phys.* **101**, 063550 (2007).
 - ¹² G. Dimonte, G. Terrones, F. J. Cherne, T. C. Germann, V. Dupont, K. Kadau, W. T. Buttler, D. M. Oro, C. Morris, and D. L. Preston, *Phys. Rev. Lett.* **107**, 264502 (2011).
 - ¹³ W. D. Reinhart, J. R. Asay, C. S. Alexander, L. C. Chhabildas, and B. J. Jensen, *J. Dyn. Behav. Mat.* **1**, 275 (2015).
 - ¹⁴ J. F. Barnes, P. J. Blewett, R. G. McQueen, K. A. Meyer, and D. Venable, *J. Appl. Phys.* **45**, 727 (1974).
 - ¹⁵ J. D. Colvin, M. Legrand, B. A. Remington, G. Shurtz and S. V. Weber, *J. Appl. Phys.* **93**, 5287 (2003).
 - ¹⁶ A. I. Lebedev, P. N. Nizovtzev, V. A. Raevsky, in *Proceedings of the Fourth International Workshop on the Physics of Compressible Turbulent Mixing*, edited by P. F. Linden, D. L. Youngs, and S. B. Dalziel (Cambridge University Press, Cambridge, England, 1993) p. 81.
 - ¹⁷ V. V. Igonin, O. N. Ignatova, A. I. Lebedev, M. O. Lebedeva, S. S. Nadezhin, A. M. Podurets, V. A. Raevsky, V. P. Solovyev, M. A. Zocher, and D. L. Preston, in *Shock Compression of*

- Condensed Matter*, Vol. 1195, edited by M. Elert, M. D. Furnish, W. W. Anderson, W. G. Proud, and W. T. Buttler (American Institute of Physics, New York, 2009) pp. 1085–1088.
- ¹⁸ V. A. Raevsky, O. N. Aprelkov, O. N. Ignatova, V. I. Igonin, A. I. Lebedev, S. S. Nadezhin, M. A. Zocher, D. Preston, and A. Kaul, *EPJ Web of Conferences* **10**, 00022 (2011).
- ¹⁹ N. R. Barton, J. V. Bernier, R. Becker, A. Arsenlis, R. Cavallo, J. Marian, M. Rhee, H. S. Park, B. A. Remington, and R. T. Olson, *J. Appl. Phys.* **109**, 073501 (2011).
- ²⁰ R. F. Smith, J. H. Eggert, R. E. Rudd, D. C. Swift, C. A. Bolme, and G. W. Collins, *J. Appl. Phys.* **110**, 123515 (2011).
- ²¹ A. R. Piriz, J. J. L. Cela, N. A. Tahir, and D. H. H. Hoffman, *Phys. Rev. E* **78**, 056401 (2008).
- ²² A. R. Piriz, J. J. L. Cela, and N. A. Tahir, *Nucl. Instrum. Meth. A* **606**, 139 (2009).
- ²³ J. W. Grove, R. Holmes, D. H. Sharp, Y. Yang, and Q. Zhang, *Phys. Rev. Lett.* **71**, 3473 (1993).
- ²⁴ B. J. Jensen, S. N. Luo, D. E. Hooks, K. Fezzaa, K. J. Ramos, J. D. Yeager, K. Kwiatkowski, T. Shimada, and D. M. Dattelbaum, *AIP Advances* **2**, 012170 (2012).
- ²⁵ S. N. Luo, B. J. Jensen, D. E. Hooks, K. Fezzaa, K. J. Ramos, J. D. Yeager, K. Kwiatkowski, and T. Shimada, *Rev. Sci. Instrum.* **83**, 073903 (2012).
- ²⁶ P. W. Bridgman, *P. Natl. Acad. Sci. USA* **8**, 361 (1922).
- ²⁷ S. Endo, H. Sasaki, and T. Mitsui, *J. Phys. Soc. Jpn.* **42**, 882 (1977).
- ²⁸ P. H. Schaufelberger, *J. Appl. Phys.* **47**, 2364 (1976).
- ²⁹ B. Sitaud, J. Pere, and T. Thevenin, *High Press. Res.* **12**, 245 (1994).
- ³⁰ A. Jayaraman, *Phys. Rev.* **137**, 179 (1965).
- ³¹ M. J. Lipp, D. Jackson, H. Cynn, C. Aracne, W. J. Evans, and A. K. McMahan, *Phys. Rev. Lett.* **101**, 165703 (2008).
- ³² E. King, J. A. Lee, I. R. Harris, and T. F. Smith, *Phys. Rev. B* **1**, 1380 (1970).
- ³³ B. J. Jensen and F. J. Cherne, *J. Appl. Phys.* **112**, 013515 (2012).
- ³⁴ G. N. Chesnut, W. W. Anderson, and J. Casson, in *Shock Compression of Condensed Matter*, edited by M. D. Furnish, M. Elert, T.P. Russell, and C.T. White (American Institute of Physics, 2006) pp. 45–48.
- ³⁵ Y. K. Vohra, S. L. Beaver, J. Akella, C. A. Ruddle, and S. T. Weir, *J. Appl. Phys.* **85**, 2451 (1999).
- ³⁶ Y. Zhao and W. B. Holzapfel, *J. Alloy. Compd.* **246**, 216 (1997).
- ³⁷ O. B. Tsiok and L. G. Khvostantsev, *J. Exp. Theor. Phys. (Russia)* **93**, 1245 (2001).

- ³⁸ A. Schiwek, F. Porsch, and W. B. Holzapfel, *High Press. Res.* **22**, 407 (2002).
- ³⁹ V. M. Elkin, V. N. Mikhaylov, A. V. Petrovtsev, and F. J. Cherne, *Phys. Rev. B* **84**, 094120 (2011).
- ⁴⁰ F. J. Cherne, *Modification to the Russian multi-phase equation of state for cerium and its associated parameters*, Tech. Rep. LA-UR-15-23933 (Los Alamos National Laboratory, 2015).
- ⁴¹ O. T. Strand, D. R. Goosman, C. Martinez, T. L. Whitworth, and W. W. Kuhlrow, *Rev. Sci. Instrum.* **77**, 083108 (2006).
- ⁴² B. J. Jensen, D. B. Holtkamp, P. A. Rigg, and D. H. Dolan, *J. Appl. Phys.* **101**, 013523 (2007).
- ⁴³ B. J. Jensen, C. T. Owens, K. J. Ramos, J. D. Yeager, R. A. Saavedra, A. J. Iverson, S. N. Luo, K. Fezzaa, and D. E. Hooks, *Rev. Sci Instrum.* **84**, 013904 (2013).
- ⁴⁴ E. J. Caramana, D. E. Burton, M. J. Shashkov, and P. P. Whalen, *J. Comp. Phys.* **146**.
- ⁴⁵ D. Burton, *A cell-centered Lagrangian hydrodynamics method for multi-dimensional unstructured grids in curvilinear coordinates with solid constitutive models*, Tech. Rep. LA-UR-11-04995 (Los Alamos National Laboratory, 2011).
- ⁴⁶ D. L. Preston, D. L. Tonks, and D. C. Wallace, *J. Appl. Phys.* **93**, 211 (2003).
- ⁴⁷ W. T. Buttler, D. M. Oro, D. L. Preston, K. O. Mikaelian, F. J. Cherne, R. S. Hixson, F. G. Mariam, C. Morris, J. B. Stone, G. Terrones, and D. Tupa, *J. Fluid Mech.* **703**, 60 (2012).
- ⁴⁸ S. J. Turneaure, Y. M. Gupta, K. Zimmerman, K. Perkins, C. S. Yoo, and G. Shen, *J. Appl. Phys.* **105**, 053520 (2009).
- ⁴⁹ S. J. Turneaure and Y. M. Gupta, *J. Appl. Phys.* **106**, 033513 (2009).

TABLE I. Relevant experimental parameters and measured and calculated quantities. Uncertainty estimates are shown in parenthesis.

Shot #	Measured Quantities				Calculated Quantities						
	V_p (km/s)	h_0 (μm)	V_{sp}^0 (km/s)	h_{sp}^{max} (μm)	P_x (GPa)	ρ (g/cc)	T_B (K)	T_C (K)	${}^2Y_{image}$ (GPa)	${}^2Y_{Vel}$ (GPa)	Y_{sim} (GPa)
	$\pm 0.1\%$	$\pm 3\mu\text{m}$	$\pm 1\%$	$\pm 3\mu\text{m}$	$\pm 1.5\%$	$\pm 3.3\%$					
13-030	0.629	51	0.311	74.1	5.62	9.297	724	489	0.15(0.011)	0.15(0.021)	0.13
13-031	0.697	51	0.364	120.8	6.50	9.453	787	518	0.13(0.007)	0.12(0.014)	0.11
13-032	0.781	51	0.373	143.9	7.64	9.638	869	557	0.11(0.006)	0.10(0.012)	0.11
13-038	0.603	76	0.337	94.9	5.30	9.243	702	478	0.14(0.009)	0.13(0.016)	0.13
13-039 ³	0.720	127	–	–	6.81	9.502	809	529	–	–	–

¹Values obtained using the measured h_{sp}^{max} in column 5.

²Values obtained using kh_{sp}^{max} determined from Eq.2.

³Some quantities for this experiment were not measured or calculated because the jet did not saturate.

FIGURE CAPTIONS

Fig. 1.: Phase diagram for cerium³⁸ showing multiple phases within a moderate pressure-temperature range along with two reported locations for the $\alpha - \epsilon$ phase boundary at higher temperatures.^{37,38} The Hugoniot is shown as red curve and represents the states accessible through shock wave loading.¹⁰ The points A, B, and C represent the ambient, shocked, and released states, respectively, which define the loading path of the sample. The blue curve represents an example calculation (experiment 13-031) showing the release from the shocked state (B) to pressures near zero (C) as the jet begins to form. The well-known critical point (CP) that terminates the $\gamma - \alpha$ boundary is indicated.

Fig. 2.: Schematic of the experimental configuration for shock wave experiments using X-ray imaging to observe jet formation in Ce. A Cu plate (2.5 mm thick) impacted the Ce sample located in an evacuated target chamber generating a shock wave that interacted with the machined perturbations at the back surface. The x-ray beam passed through multiple slits and shutters, interacted with the sample and evolving jets, and was incident upon a scintillator. The scintillator light was imaged onto four optically multiplexed intensified detectors which were synchronized to the impact event and the X-rays. (inset) Schematic showing the process of jet formation as the shock wave interacted with the groove in the sample.

Fig. 3.: (A) Example X-ray images showing jet formation for shot 13-030. The image is a convolution of the initial static groove image (F_0) and five additional frames (F_1 to F_5) at 153.4 ns intervals. Line outs of the groove and jet interfaces were obtained using an edge finding algorithm and plotted on the image. (B) Corresponding velocimetry data (black curves) obtained using PDV showing the jet and free surface velocities. Simulated histories obtained from the continuum code FLAG are shown as blue curves. All curves were arbitrarily shifted so that shock arrival occurred at time $t = 0$. (C) A summary of X-ray images for five experiments showing the effect of increasing the impact stress and groove depth on the jet formation. For the deepest grooves, the jet does not saturate and outruns the free surface. All images are shown in false-color for clarity.

Fig. 4.: FLAG Calculations for shot 13-030 with appropriate models for Cu and Ce and a simple deviatoric strength model. The initial sample geometry with the groove is shown in (A). The results for three simulations (plotted 950 nanoseconds after shock breakout) showing the shape of the jet for various values of the yield stress , Y_{sim} , are shown in (B) $Y_{sim} = 0.26$, (C) $Y_{sim} = 0.13$, and (D) $Y_{sim} = 0.065$ GPa. The colormap The shape in (C) best fits the experimental data shown in Figure 3A. The simulations show that small changes in Y lead to significant variation in jet height.

Fig. 5.: FLAG Calculations using the yield stress value for shot 13-030 showing the shock wave propagation through the material and subsequent evolution of the jet with time. The colormap represents the normal stress. (A) A 5.62 GPa shock wave (peak values are slightly off scale) is shown interacting with the perturbations at the cerium-vacuum interface. (B-D) The shock wave reflects from the cerium-vacuum interface causing the formation of jets and begins propagating back into the sample as a release wave.

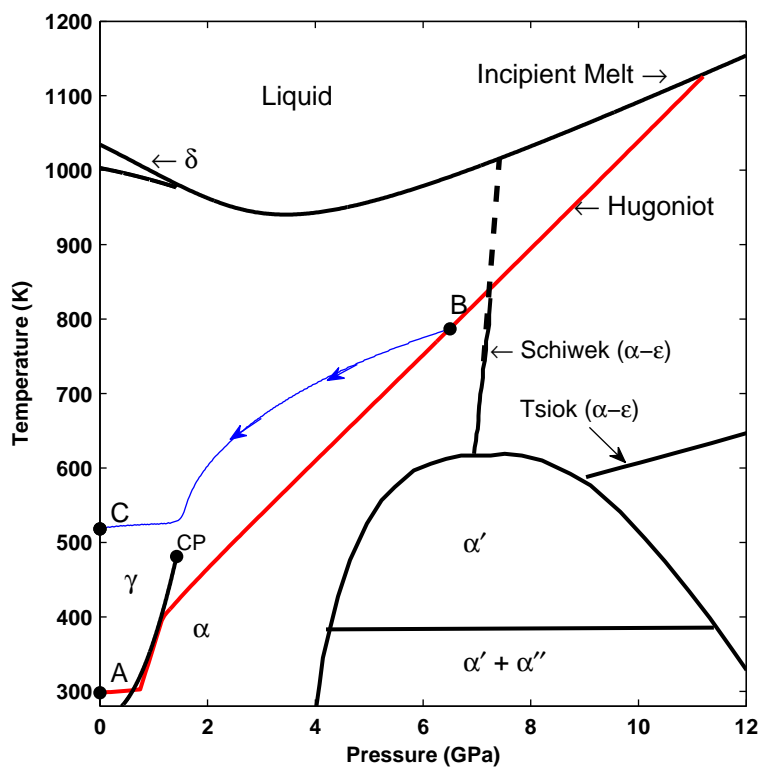


Fig. 1, B.J. Jensen, J. Appl. Phys.

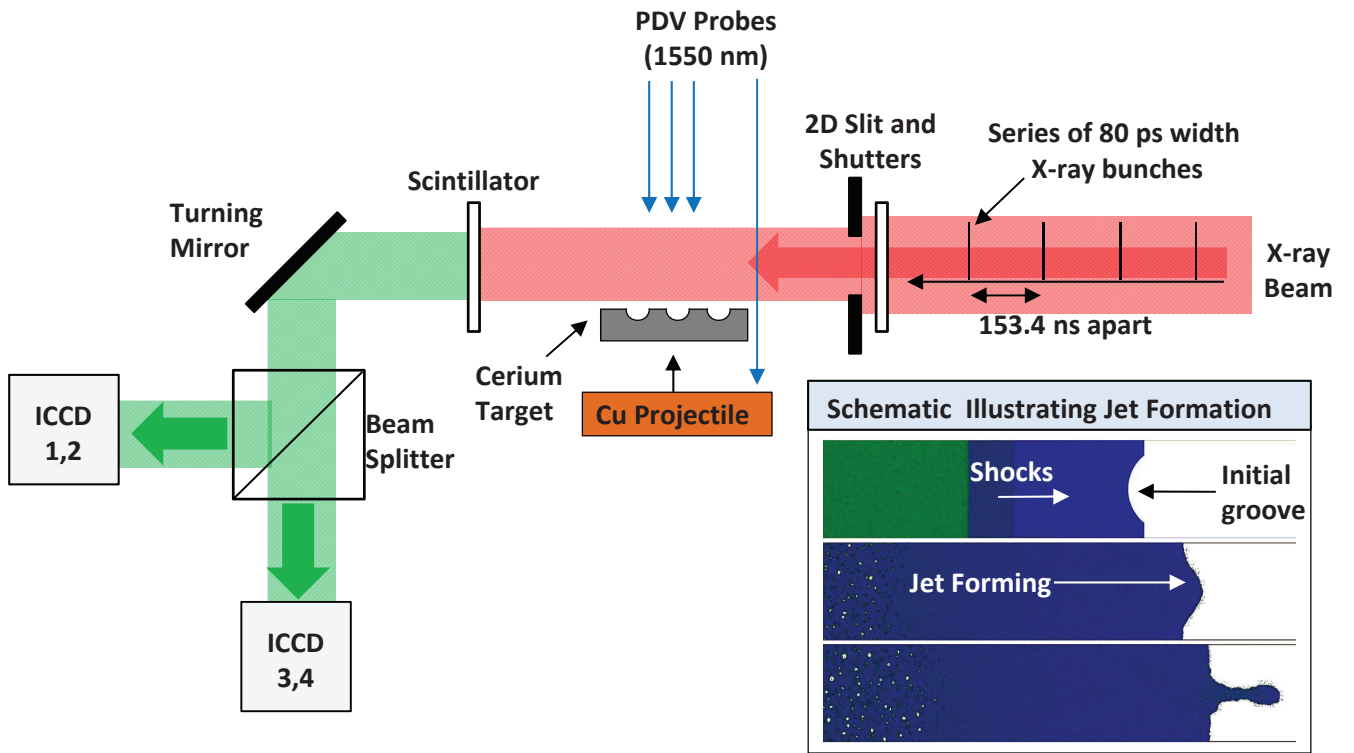


Fig. 2, B.J. Jensen, J. Appl. Phys.

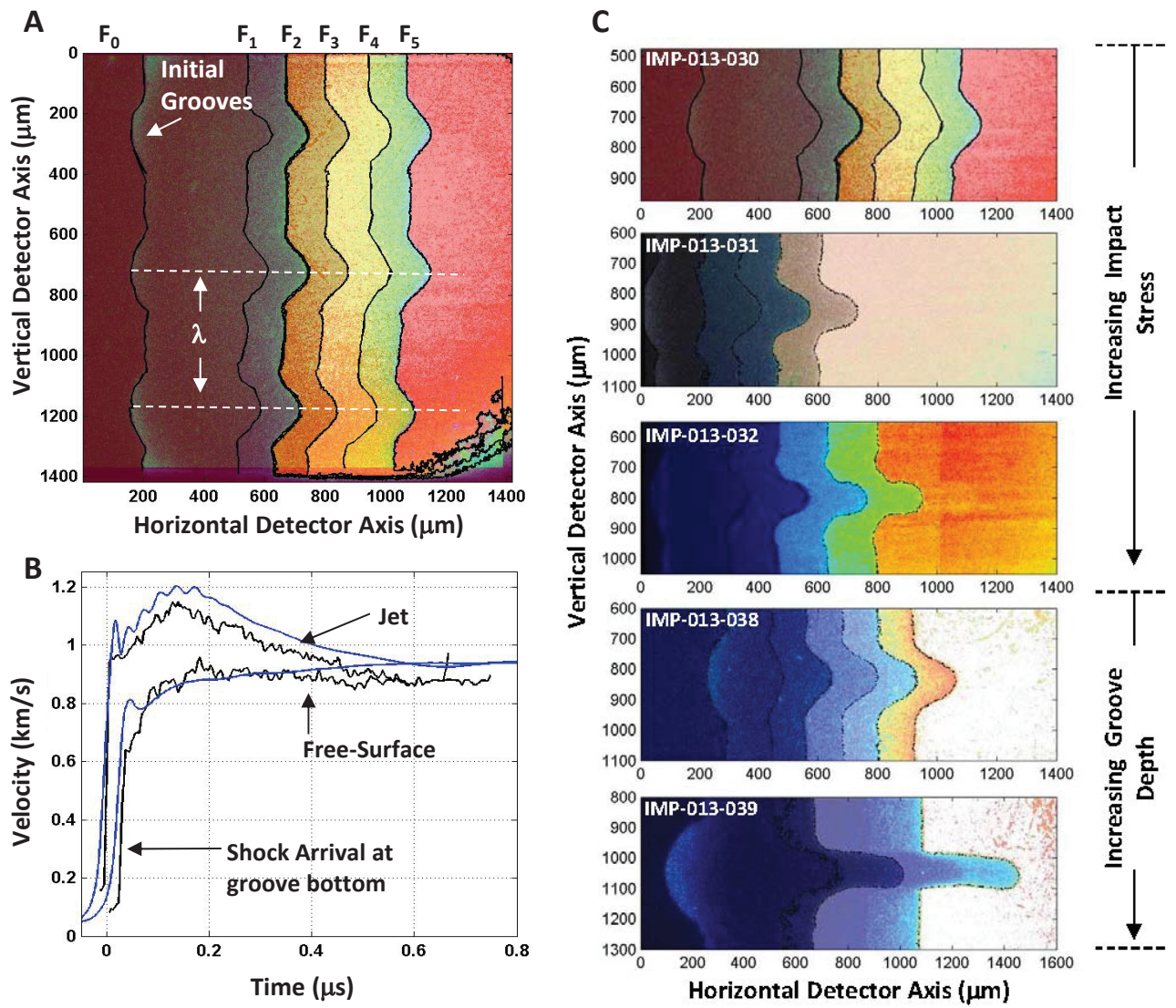


Fig. 3, B.J. Jensen, J. Appl. Phys.

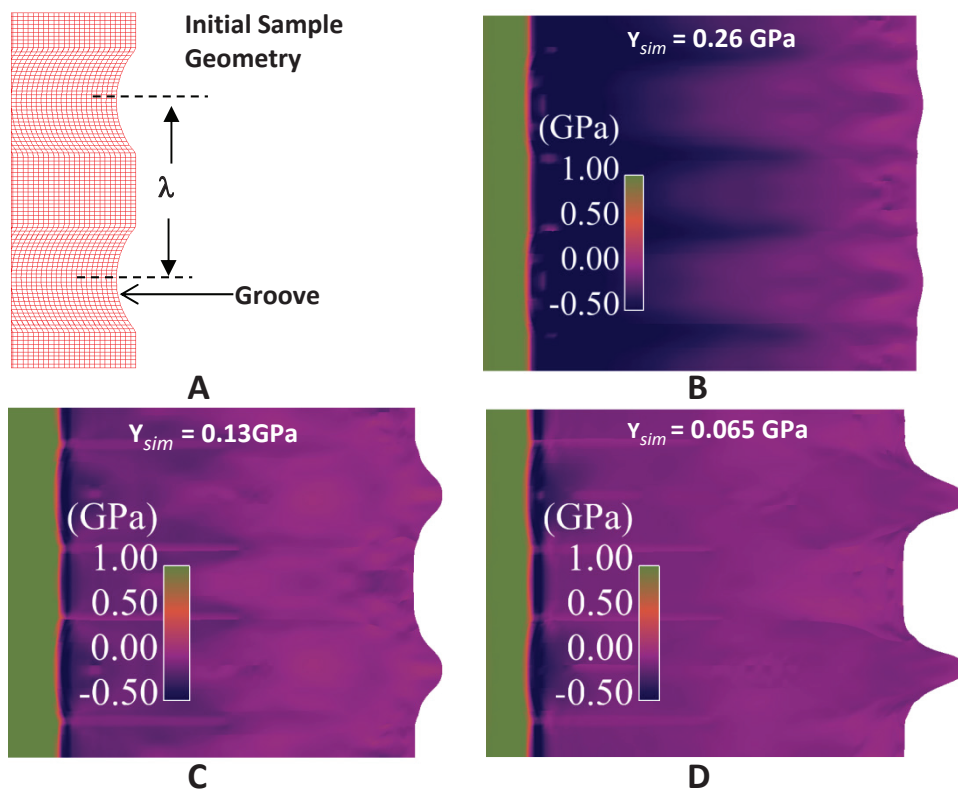


Fig. 4, B.J. Jensen, J. Appl. Phys.

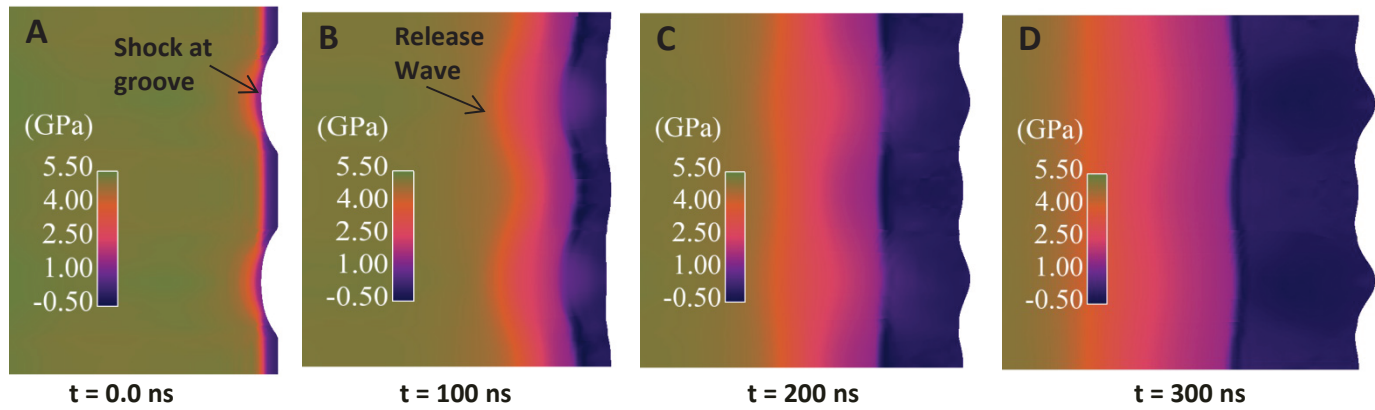


Fig. 5, B.J. Jensen, J. Appl. Phys.